DYNAMIC ANALYSIS OF A NEW CONNECTION FOR DUAL VOLTAGE OPERATION OF SINGLE PHASE CAPACITOR RUN MOTOR

H. H. Hanafy
Electrical power and machines Dept., Faculty of Engineering, Cairo University, Giza-Egypt.
Add.: Electrical power and machines dept., Faculty of Engineering, Cairo University, Giza-Egypt, Zip 12613.
e-mail: Hanafy_Hassan@hotmail.com

Abstract: *This paper presents the dynamic analysis of a new connection of Single-Phase Capacitor Run Motor (SPCRM) for dual voltage operation. A program simulating the dynamic behavior of the new connection in the stationary d-q reference frame gives sufficient results. The analysis is carried out under the no-load and load conditions. Experimental measurements are carried out for comparison and verification of simulating results. The agreement of experimental and computational results approves the dynamic model of the new connection.*

Key words: *Single phase induction motor, capacitor run motor, dynamic analysis, dual voltage.*

Nomenclature

r_{1m}	main winding resistance;
r_{1a}	auxiliary winding resistance;
r_r	rotor windings resistance referred to the main winding;
L_o	magnetizing inductance referred to the main winding;
L_{lm}	main winding leakage inductance ;
L_{la}	auxiliary winding leakage inductance;
L_{lr}	rotor windings leakage inductance referred to the main winding;
i_m	main current;
i_a	auxiliary current;
$i_{\alpha r}$	rotor current of phase α;
$i_{\beta r}$	rotor current of phase β;
i_{dr}	direct component of rotor current;
i_{qr}	quadrature component of rotor current;
v_m	main voltage;
v_a	auxiliary voltage;
v_C	voltage across the capacitor;
P	number of pole-pairs;
J	moment of inertia (kg·m2);
B_f	viscous friction coefficient (N·m/(rad/s))
ω	electrical angular velocity of the rotor;
T_L	load torque;
n	motor speed;
p	differential operator w.r.t. time.

1. Introduction

Single-phase induction motors are widely used because of their cost, reliability and robustness in operation. Single phase capacitor motors operate either as “capacitor run motor”, where the auxiliary winding is permanently energized, or as “capacitor start motor”, where the auxiliary winding is switched out of circuit, or finally as “capacitor start capacitor run motor”, where the value of the capacitor is large during starting and small during running.

The single phase capacitor run motors (SPCRM) are used for many applications such as heating, ventilating and air conditioning (HVAC) blowers and compressors. The SPCRM has many advantages such as moderated starting torque and good running performance (high out power, high power factor, high efficiency and low supply current)[1].

The dual voltage operation of the SPCRM is commonly since the mains electricity in Europe, Australia, most regions of Africa and Asia and few countries in South America use the voltage of (220/240 V, 50 Hz), while most of the North American countries use (110/127 V, 60 Hz).

The author in [2] presented the theory of operation and the steady state analysis of a new connection of the SPCRM (as shown in Fig.1) for dual voltage operation as well as for supplying the SPCRM with the line-to-line voltage instead of the line-to-neutral voltage of the same grid in case of missing the neutral point, and showed that the suggested connection has a satisfactory performance and overcomes the disadvantages of the conventional dual voltage connections given in [3-4].

Through this paper the transient analysis of the new connection will be carried out. The transient analysis of the electric motors is very essential because it helps in determining the insulation strength, suitability of winding, shaft strength, value of capacitor, and devising the protection strategy.

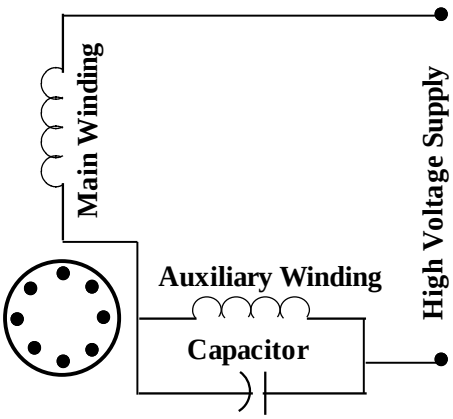

Fig. 1 The new connection of the SPCRM

Dynamic simulation of electrical machines is performed by several methods, and it is mostly based on the d-q model [5]. Tichenor et al. [6] presented a multiple reference frame based model of a generically configured permanent split capacitor induction machine. The model was valid for both steady state and transient analysis. In [7] the authors applied the dynamic phasor methodology to modeling of a single-phase induction machine with a position dependent load. The developed dynamic model of the machine predicted its transients well, and could be used in high performance control algorithms. Sadowski et al. [8] carried out the dynamic operation of a single phase induction motor using a general method coupling field and electrical circuit equations. Simulation of a single-phase induction machine using 2-D finite elements method was presented in [9]. Also there are many available software packages for the analysis of the electric machines such as EMTP and PSPICE. The authors in [10] investigated the transient phenomena of capacitor induction machines, where the machine equations were evaluated using a power system package Electromagnetic Transients Program (EMTP) Universal Machine (UM) modeling. Jawad et al. [11] investigated the dynamic Analysis of a single-phase induction motor using PSPICE and compared the results with that obtained by EMTP, showing the advantages of using PSPICE over EMTP.

This paper presents the dynamic analysis of the new connection of the SPCRM for dual voltage operation under no load and load conditions. The simulation results obtained were proved experimentally in the laboratory by loading the SPCRM using a dynamometer.

2. Mathematical Model

The mathematical model of the SPCRM will be constructed in the stationary d-q frame. Fig. 2 shows the configuration of the SPCRM, where the squirrel cage rotor may be represented as a pair of symmetrical and orthogonal, short-circuited coils (α_r, β_r). Since the axes of the stator windings are orthogonal, the d-q axes of the model may be aligned with axes of the windings, as illustrated in Fig. 2. The stator variables remain unchanged because there is no transformation on these variables. The transformation used to transform the rotor variables to the stationary d-q frame is given in (1).

$$\begin{bmatrix} i_{\alpha r} \\ i_{\beta r} \end{bmatrix} = \begin{bmatrix} \cos\theta & \sin\theta \\ -\sin\theta & \cos\theta \end{bmatrix} \begin{bmatrix} i_{dr} \\ i_{qr} \end{bmatrix} \quad (1)$$

The dynamic model of the new connection of the SPCRM in the stationary d-q frame can be described by set of differential equations, written in the matrix form as follows:

$$\begin{bmatrix} v_m \\ v_a \\ 0 \\ 0 \end{bmatrix} = \begin{bmatrix} r_{1m} + pL_{mm} & 0 & pL_o & 0 \\ 0 & r_{1a}a^2 + pL_{aa} & 0 & pL_o \\ pL_o & \theta^{\bullet}L_o & r_r + pL_{rr} & \theta^{\bullet}L_{rr} \\ -\theta^{\bullet}L_o & pL_o & -\theta^{\bullet}L_{rr} & r_r + pL_{rr} \end{bmatrix} \begin{bmatrix} i_m \\ i_a^{/} \\ i_{dr} \\ i_{qr} \end{bmatrix} \quad (2)$$

$$v_s = v_m + v_a \quad , \quad v_a = v_c \quad (3)$$

$$i_m = i_c + i_a \quad (4)$$

$$i_c = C\, p v_a \quad (5)$$

The mechanical equations which represent the dynamics of the mechanical system can be written as:

$$T_{em} = PL_o(i_a^{/} i_{dr} - i_m i_{qr}) \quad (6)$$

$$p\omega = \frac{P}{J}(T_{em} - B_f\omega - T_L) \quad (7)$$

$$p\theta = \omega \quad (8)$$

Where:

$L_{mm} = L_{lm} + L_o$

$L_{aa} = a^2 L_{la} + L_o$

$L_{rr} = L_{lr} + L_o$

$i_a^{/} = a\, i_a$

a = the effective turns ratio of the auxiliary winding to the main winding.

T_{em} = the electromechanical torque of the motor.

θ = angular displacement of the rotor w.r.t. the stator.

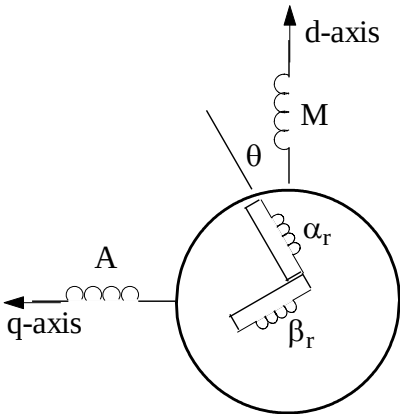

Fig. 2 The configuration of the SPCRM

3. Simulation Results

The dynamic simulation of the new connection is carried out using a capacitor run single-phase induction motor with the following specifications: 175 W, 220 V, 50 Hz, 1440 rpm, 1.5 A, and a 10 µF capacitor. Table1 gives the experimentally determined parameters of the motor.

The operation of the new connection is studied by a supply voltage of 380 V-50 Hz to the motor configuration shown in Fig. 1.

Table 1 Parameters of the SPCRM

Parameter	Value
r_{1m}	26 Ω
r_{1a}	24 Ω
L_{lm}	0.0871 H
L_{la}	0.067 H
r_r	14.32 Ω
L_{lr}	0.087 H
L_o	0.9022 H
J	0.0035 Kg.m^2
B_f	0.003 N·m/(rad/s)
a	1.0235

3.1. No-Load Conditions

The simulation results in this section are obtained for free acceleration of the motor with zero load torque. Only the moment of inertia of the motor "J" and the viscous friction coefficient "B_f" were taken into account.

Fig. 3 shows the speed time curve, where the acceleration period ends at approximately one sec. and the motor reaches its no load speed of 1490 rpm.

Figs. 4-5 show the main winding and the auxiliary winding currents with time; it is clear that the currents decrease to their steady state values as the motor attains the no load speed. Figs. 6-7 represent the main winding and the auxiliary winding voltages versus time; it is clear that the voltages remain nearly constant at low speeds until the speed has reached the steady state value then they increase to their steady state value as the motor attains the no load speed.

Fig. 8 illustrates the rotor phase current against time; it is obvious that the rotor current has high values and frequency during the acceleration period and low value and very low frequency at steady state due to the operating slip.

Fig. 9 shows the variation of the electromagnetic torque of the motor; it can be observed very high oscillations of torque at twice supply frequency which influence on pulsations of the speed. These oscillations are caused by elliptical rotating field due to the phase difference between the main and auxiliary windings currents and also the unequal amplitudes of these currents. The elliptical shape of the rotating magnetic field can be observed in the trajectory of the stator currents shown in Fig. 10

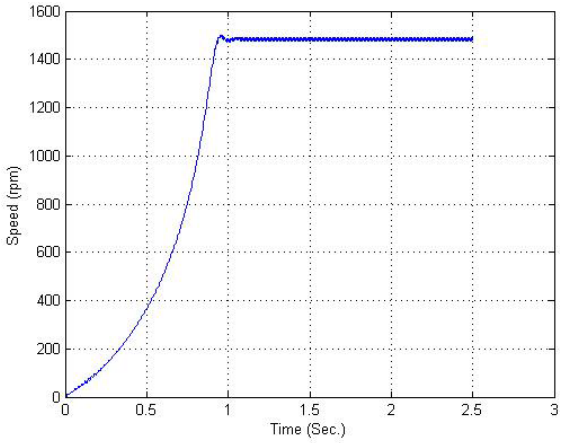

Fig. 3 The speed time curve at no load

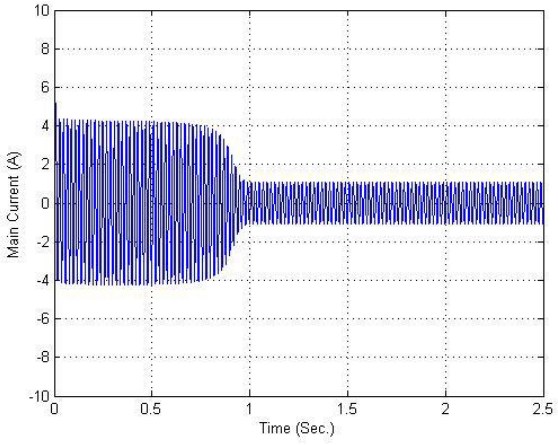

Fig. 4 The main current versus time at no load

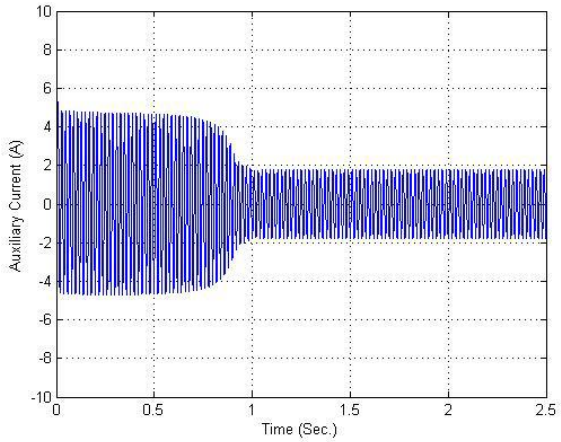

Fig. 5 The auxiliary current versus time at no load

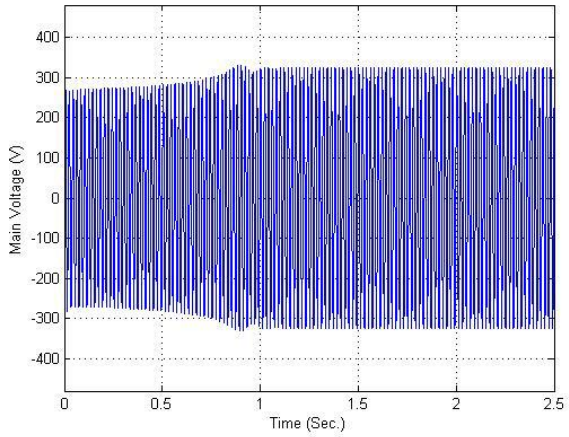

Fig. 6 The main voltage versus time at no load

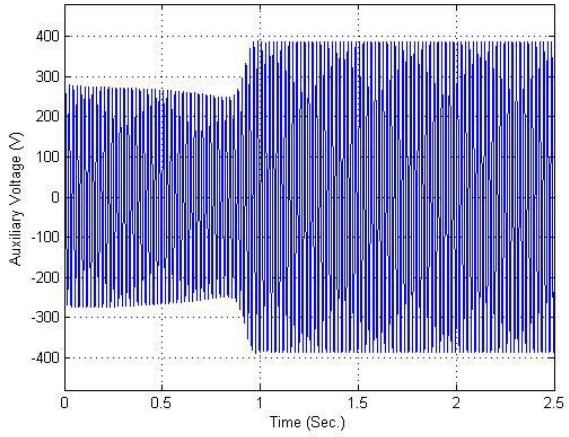

Fig. 7 The auxiliary voltage versus time at no load

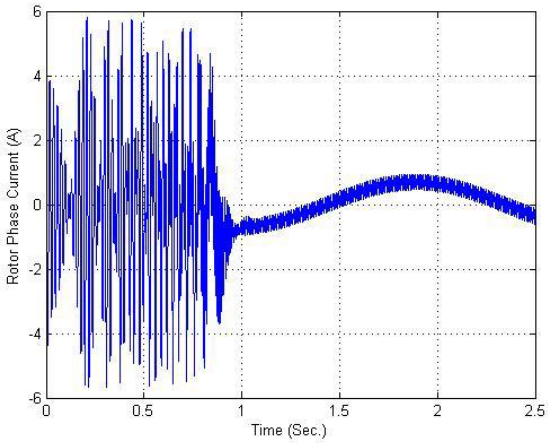

Fig. 8 The rotor phase current versus time at no load

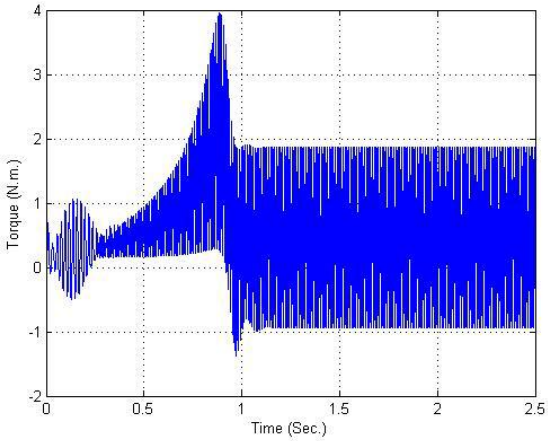

Fig. 9 The electromagnetic torque versus time at no load

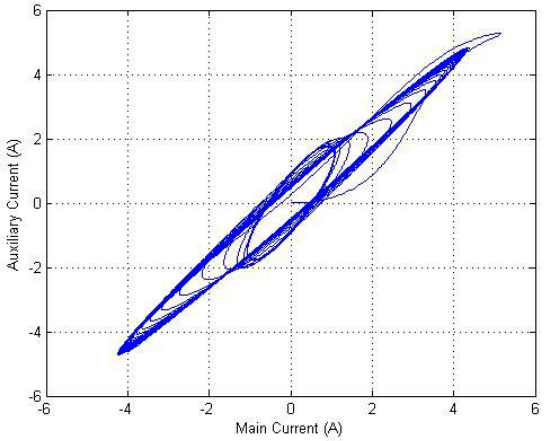

Fig. 10 Trajectory of the stator currents at no load

3.2. Load Conditions

The simulation results in this section are obtained at load conditions by applying a load torque of 1.0 N·m (approximately 85% of the full load torque) after 2.5 sec.

Fig. 11 shows the speed time curve, it can be noticed, that the speed decreases from the no load value of 1490 rpm to 1430 rpm at load conditions.

Figs. 12-13 show the main winding and the auxiliary winding currents with time; it can be observed that the main current increases with loading, while the auxiliary current slightly decreases.

Figs. 14-15 represent the main winding and the auxiliary winding voltages versus time; it is clear that the main voltage remains nearly constant with loading, while the auxiliary voltage decreases.

Fig. 16 demonstrates the rotor phase current against time; it is obvious that the amplitude and the frequency of the rotor current increase with loading due to the high operating slip. Also it can be noticed, that the rotor current has oscillations, which are caused by the pulsations of the speed due to oscillations of the electromagnetic torque.

Fig. 17 shows the variation of the electromagnetic torque of the motor. The electromagnetic torque is composed of the steady state time averaged torque and the double frequency pulsating torque. The pulsating torque produces noise and vibration during running, while the average torque is responsible for overcoming the friction and driving the load. This double-stator frequency torque oscillations are produced by the interaction of oppositely rotating mmf waves which relatively rotate to each other at twice the synchronous speed.

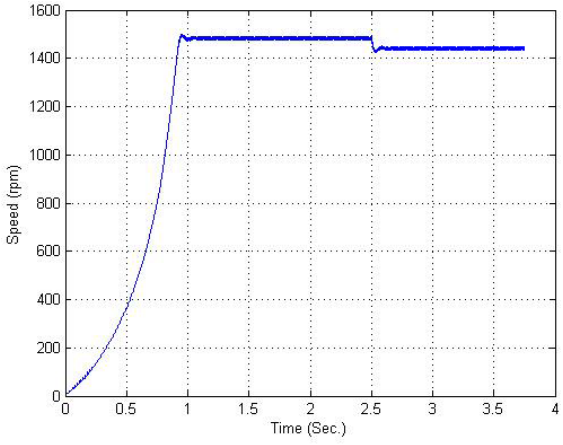

Fig. 11 The speed time curve at load conditions

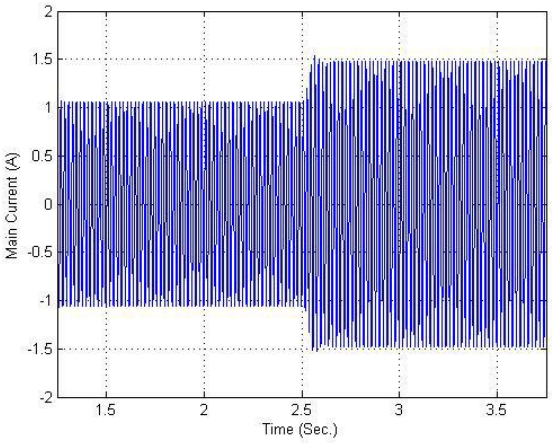

Fig. 12 The main current versus time at load conditions

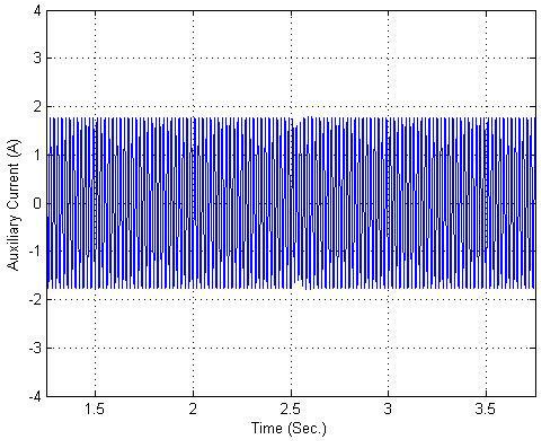

Fig. 13 The auxiliary current versus time at load conditions

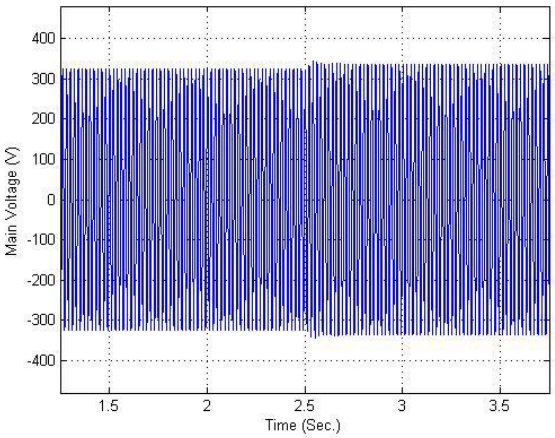

Fig. 14 The main voltage versus time at load conditions

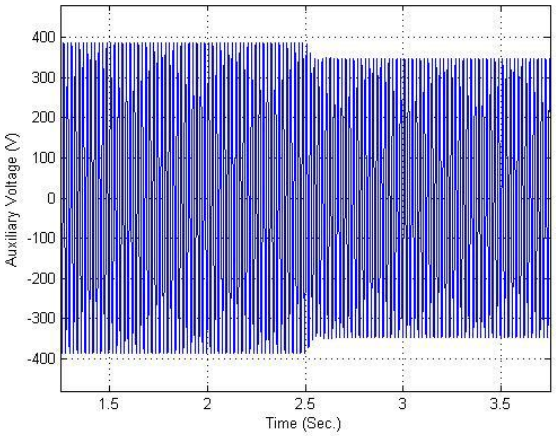

Fig. 15 The auxiliary voltage versus time at load conditions

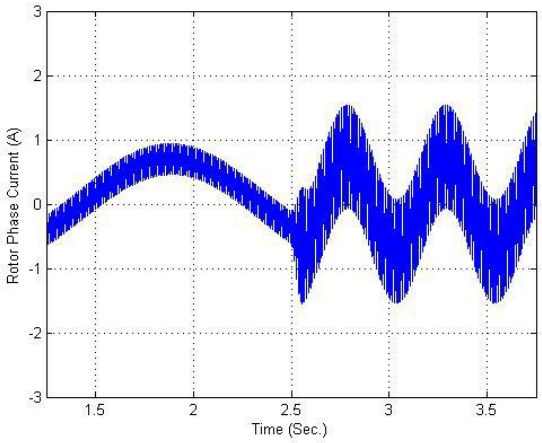

Fig. 16 The rotor phase current versus time at load conditions

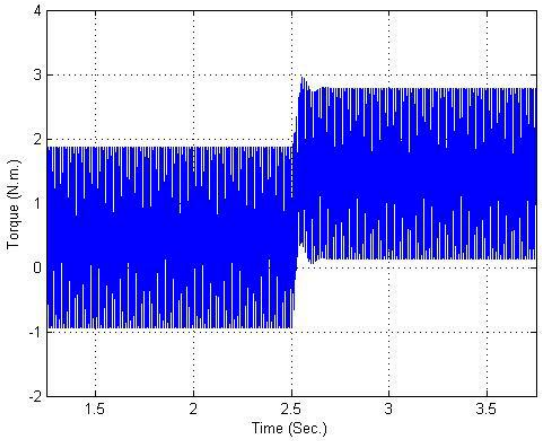

Fig. 17 The electromagnetic torque versus time at load conditions

4. Experimental Results

The new connection of the SPCRM is tested and in the laboratory by mechanically coupling the SPCRM to a dynamometer, where the load torque could be electrically controlled. The speed is recorded using a DC tachometer with a gain of 1V/500 rpm. The currents and voltages waveforms are recorded using dual-channel digital oscilloscope through current and voltage transducers. Table 2 gives the specifications of the transducers.

Table 2 Specifications of the transducers

Transducer	Input signal	Output signal
Current	0-5 A	0-10 V
Voltage	0-600 V	0-10 V

4.1. No Load Results

The experimental results in this section are obtained for free acceleration of the motor with zero load torque. Fig. 18 shows the speed time curve. Figs. 19-20 show the main winding and the auxiliary winding currents with time. Figs. 21-22 give the main winding and the auxiliary winding voltages versus time.

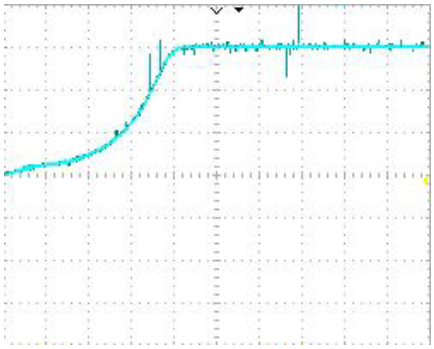

Fig. 18 The experimental speed time curve at no load (1 V/Div. & 0.25 Sec./Div)

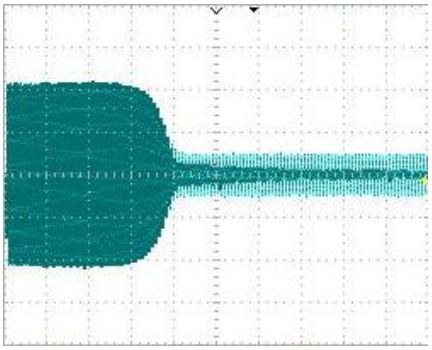

Fig. 19 The experimental main current versus time at no load (2.5 A/Div. & 0.25 Sec./Div)

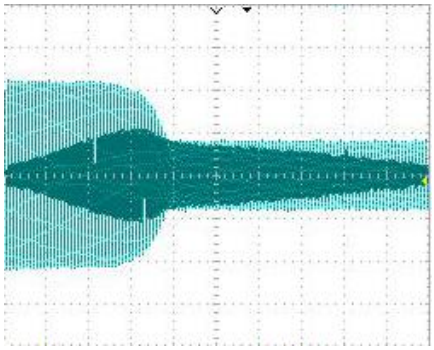

Fig. 20 The experimental auxiliary current versus time at no load (2.5 A/Div. & 0.25 Sec./Div)

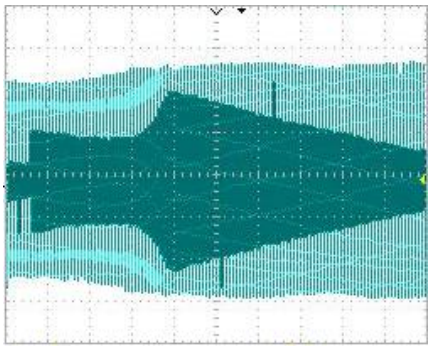

Fig. 21 The experimental main voltage versus time at no load (120 V/Div. & 0.25 Sec./Div)

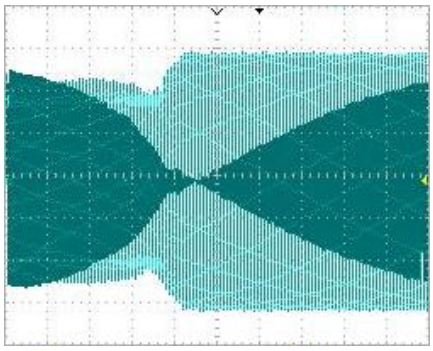

Fig. 22 The experimental auxiliary voltage versus time at no load (120 V/Div. & 0.25 Sec./Div)

4.2. Load Results

The experimental results in this section are obtained at load conditions by applying a load torque of 1.0 N·m; after the motor reaches its steady state no load speed. Figs. 23-24 show the main winding and the auxiliary winding currents with time; it can be observed that the main current increases with loading, while the auxiliary current slightly decreases.

Figs. 25-26 represent the main winding and the auxiliary winding voltages versus time; it is clear that the main voltage remains nearly constant with loading, while the auxiliary voltage decreases.

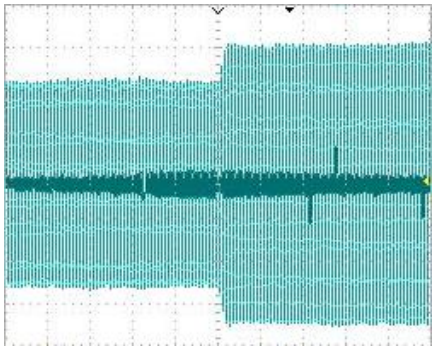

Fig. 23 The experimental variation of the main current versus time with load (0.5 A/Div. & 0.25 Sec./Div)

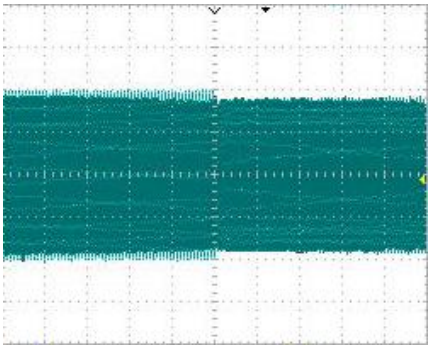

Fig. 24 The experimental variation of the auxiliary current versus time with load (1.0 A/Div. & 0.25 Sec./Div)

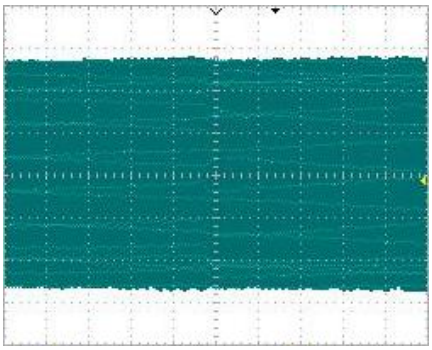

Fig. 25 The experimental variation of the main voltage versus time with load (120 V/Div. & 0.25 Sec./Div)

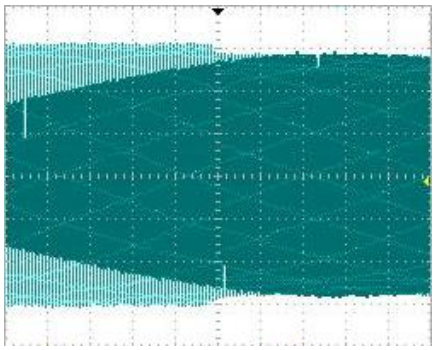

Fig. 25 The experimental variation of the auxiliary voltage versus time with load (120 V/Div. & 0.25 Sec./Div)

By comparing the results of sections 3 & 4; one can conclude that, the simulations waveforms are very close to those obtained from the experimental results. The small differences between the simulation and the experimental results can be explained as a result of neglecting the core losses, effect of the temperature and effect of the saturation in the mathematical dynamic model.

5. Conclusions

In this paper, the dynamic analysis of a new connection for operating the SPCRM from dual voltage, in the stationary d-q frame, has been presented. Experimental work has been carried out to examine the proposed mathematical dynamic model for the new connection of the SPCRM and to ensure the accuracy of computational technique under different operating conditions. Experimental results show correctness and validity of the presented mathematical dynamic model of the SPCRM.

The results show that all voltages and currents of the motor windings are within the safe limits during the starting, no load and load conditions.

References

1. Yeadon W. H., Yeadon A.W.: *Handbook of small electric motors*. McGraw-Hill, 2001.

2. Hanafy H. H.: *Performance Prediction of a New Connection for Dual Voltage Operation of Single Phase Capacitor Run Moto.* In: Journal of Electrical Engineering (JEE) , vol.12, no.2, July 2012,p. 185-191.

3. Jim Cox: *Electric Motors*. p. 39-42, Argus Books Ltd 1988.

4. Hans-Dieter Stölting, Eberhard Kallenbach, Wolfgang Amrhein: *Handbook of Fractional-Horsepower Drives*, p.134-140, Springer Verlag, Berlin, Heidelberg, New York, 2008.

5. Krause P. C., Wasynczuk O., and Sudhoff S. D.: *Analysis of Electric Machinery*. IEEE Press, New York, 1995.

6. Tichenor J.L., Chapman P.L., Sudhoff S.D. and Budzynski R.: *Analysis of Generically Configured PSC Induction Machines.* In: IEEE Trans. on Energy Conversion, vol. 14, no. 1, March 1999, p. 108-114.

7. Stankovic A.M. and Liu H.: *Modeling, Analysis and Simulation of Single Phase Induction Machines With Position-Dependent Loads*. In: IEEE Nordic Workshop on Power and Industrial Electronics, NORPIE 2000, June 2000, p. 27-31.

8. Sadowski N., Carison R., Arruda S.R., da Silva C.A. and Mazenc M. L.: *Simulation of Single Phase Induction Motor by a General Method for Coupling Field and Circuit Equations.* In: IEEE Trans. Magns., vol. 31, no.3, May 1995, p. 1908–1911.

9. Rajanathan C. and Watson B.: *Simulation of a single-phase induction motor operating in the motoring, generating, and braking modes*. In: IEEE Trans. Magns., vol. 32, May 1996, p. 1541–1544.

10. Alexander Domijan, **Jr,** and Yuexin Yin: *Single Phase Induction Machine Simulation Using The Electromagnetic Transients Program: Theory And Test Cases*. In: IEEE Trans. on Energy Conversion, vol. 9, no. 3, September 1994, P. 535-542.

11. Jawad Faiz and Keyhani A.: *PSPICE Simulation of Single Phase Induction Motors*. In: IEEE Trans. on Energy Conversion, vol. 14, no. 1, March 1999, p. 86-92.